Fractals, Multifractals, and Thermodynamics

An Introductory Review *

Tamás Tél
Institute for Theoretical Physics, Roland Eötvös University, Budapest, Hungary

Z. Naturforsch. **43a**, 1154–1174 (1988); received February 9, 1988, in revised form September 2, 1988

The basic concept of fractals and multifractals are introduced for pedagogical purposes, and the present status is reviewed. The emphasis is put on illustrative examples with simple mathematical structures rather than on numerical methods or experimental techniques. As a general characterization of fractals and multifractals a thermodynamical formalism is introduced, establishing a connection between fractal properties and the statistical mechanics of spin chains.

I. Fractals

1. Introduction

The surface-to-volume ratio for usual macroscopic bodies (sphere, cube, etc.) is small since this ratio is inversely proportional to the linear size of the system, and the latter is characterized by a large number in appropriate (atomic) units. There exist, however, porous or hairly objects with a large surface-to-volume ratio. They may play a fundamental role in natural phenomena. Efficient catalysis, e.g., requires materials with large surface area. The need of a rapid gas exchange explains the existence of the large surface-to-volume ratio observed in the lung. The area of the human lungs respiratory surface (measured with the resolution of 100 μm) is as large as that of a tennis-court (of order 10^2 m^2) while the volume enclosed by it is of a few litres [1] (of order 10^{-3} m^{-3}). The general importance of such systems was recognized by B. Mandelbrot. He also coined the name *fractal* and worked out a new type of geometry for their mathematical description [2]. (For further references on fractals, see [3–9]).

The following observation leads to a broad definition of fractals: Experience shows that in such systems the *surface area depends on the resolution* used in the measurement. Typically, this area diverges as the resolution is increased. The area of usual objects also depends on the resolution but it converges very fast to a finite limiting value. In the case of fractals the resolution dependence can, however, be followed over *several* orders of magnitude. Since not only surfaces or curves can be fractals but also dust-like objects, it is useful to extend the definition by introducing the concept of the *observed volume*. Let $d=1, 2, 3$ denote the Euclidean dimension of the geometric entity the set of interest is embedded in. (More precisely, d should be the smallest possible such dimension.) For a fixed *grid* of d-dimensional cubes of size l the observed volume $V(l)$ is the total volume of the boxes needed to cover the object, i.e. of boxes containing part of the set (Fig. 1). An object will be called fractal if its *observed volume depends on the resolution* (grid size) *over several orders of magnitude and follows a power law behaviour* with a nontrivial exponent. This dependence can be observed over an infinite range of the resolution in the case of fractals generated by mathematical constructions. Such fractals have no smallest or no largest scale.

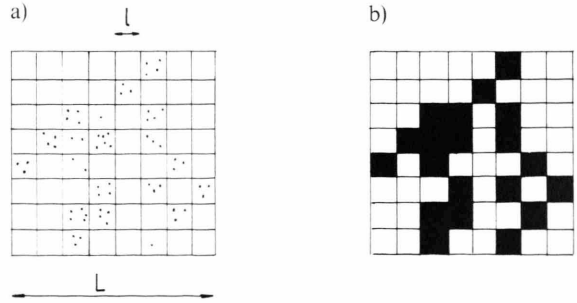

Fig. 1. a) A set (dots) and a grid of size l. L denotes the diameter of the set. b) Boxes (black) needed to cover the set.

* Chapters I and II are based on a talk given at the Winter School on Fractals, Budapest, January 12–16, 1987.

Reprint requests to Tamás Tél, KFA, IFF, Pf. 1913, D-5170 Jülich 1 (address for 1989).

0932-0784 / 88 / 1200-1154 $ 01.30/0. – Please order a reprint rather than making your own copy.

2. Fractal Dimension

It is intuitively appealing to think of a hairly surface as an object of dimension larger than 2. More ramified surfaces should have larger dimensions. This idea is formulated in a quantitative manner by the concept of the *fractal dimension* [2].

Let L be the diameter (more generally, a characteristic linear size) of the set to be investigated. Using the aforementioned grid of box-size l, the number of cubes needed to cover the set is denoted by $N(l, L)$ (Figure 1). This number can depend only on a dimensionless quantity which must be

$$\varepsilon = l/L\,, \tag{1}$$

i.e. the box-size expressed in units of L. Therefore, we have $N(l, L) \equiv N(\varepsilon)$. The number of nonempty cubes increases with a decresing box-size.

It is easy to find the precize form of $N(\varepsilon)$ for usual geometric objects. As a simple example, we consider first a straight line segment of length L. Let us use a grid obtained by dividing the segment into equal pieces of length l. Their number is obviously L/l. Thus, $N(\varepsilon)=\varepsilon^{-1}$ for a straight line segment. In the more general case of compact d-dimensional objects (like a sphere) $N(\varepsilon) \sim \varepsilon^{-d}$ is obtained, provided the box size l is sufficiently small, since the volume of such bodies goes with the d-th power of their linear size L. The symbol $\sim$ means here and in the following that the proportionality constant, not written out explicitly, is independent of the resolution.

Next, we show that the rule found for compact object must be modified for noncompact ones. Let us consider the so-called triadic Cantor set [10, 2] which is constructed as follows. One begins with the unit interval. The middle third of the interval is removed, leaving two intervals of length 1/3. Next one removes the middle third of each of these two intervals, leaving four intervals of length 1/9, and this is then repeated with the remaining pieces again and again (Figure 2). The Cantor set is then the set of the points *not* removed by this procedure. Let us use a grid obtained by dividing the unit interval into 3^m equal intervals (m is a fixed integer). As follows from the construction, the number of such pieces (of size 3^{-m}) needed to cover the Cantor set is 2^m. Since $L = 1$ we have $\varepsilon = l = 3^{-m}$. Consequently, $N(\varepsilon) = 2^m = \varepsilon^{-\ln 2/\ln 3} = \varepsilon^{-0.631}$.

The example illustrates the general finding that $N(\varepsilon)$ exhibits a power-law behaviour also for noncompact objects. The exponent is, however, *not an integer* and is smaller than the Euclidean dimension of the space the object is embedded in.

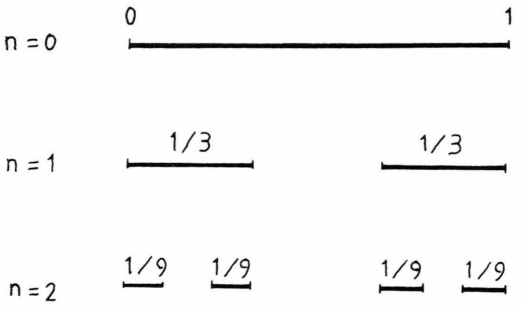

Fig. 2. The first steps in constructing the triadic Cantor set. For the resulting fractal $D_0 = 0.631$.

Thus, the following definition seems to be quite plausible. Let us consider the ε-dependence of $N(\varepsilon)$ for an arbitrary object at sufficiently fine resolution. The relation

$$N(\varepsilon) \sim \varepsilon^{-D_0}\,, \tag{2}$$

with $\varepsilon \ll 1$, defines a positive quantity D_0, the so-called *fractal dimension.* (It is worth noting that there exist also other variants in the definition of fractal dimension [2, 3, 5].)

Remarks:

1. Fractals obtained from mathematical constructions can be divided into two main classes according to their rule of construction. To the first class belong fractals generated by defining structures on finer and finer scales (see the triadic Cantor set and Examples I, III below). Consequently, such fractals *have no smallest scale.* In this case $L = \text{const}$, and (1) and (2) imply

$$N(l, L) \sim l^{-D_0}. \tag{2a}$$

In order to model aggregation-like phenomena, fractals constructed by *growth processes* (Examples II, IV) are used. Then the grid size l can be kept constant, and D_0 is to be deduced from the relation *

$$N(l, L) \sim L^{D_0}\,. \tag{2b}$$

* If l is proportional to the particle size, $N(l, L)$ becomes proportional to the mass $M(L)$ of the cluster with diameter L. Thus $M(L) \sim L^{D_0}$ follows, which is a widely used relation for growth processes.

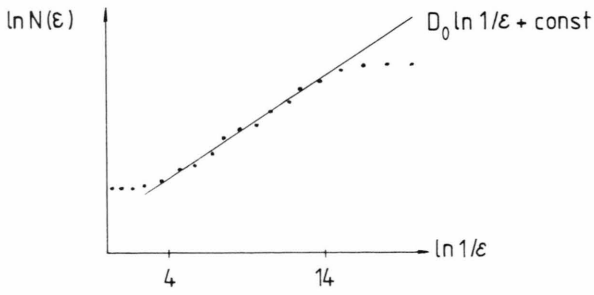

Fig. 3. A typical $\ln N(\varepsilon)$ vs. $\ln(1/\varepsilon)$ plot.

The resulting fractals *have no largest scale*. By an appropriate rescaling of the linear size, however, this second class can be made equivalent to the first one. This is exactly the physical meaning of the fact that the number of nonempty cubes depends only on the ratio ε.

2. Since $N(\varepsilon)$ cannot be larger than the number of cubes needed to fill the space, $D_0 \leqq d$ is obtained. For compact geometrical objects, (2) holds with the Euclidean dimension, $D_0 = d$.

3. It has been mentioned that ε must be much smaller than unity in (2). In physical examples, there exists also a *lower* cut-off for ε since the fractal structure is replaced by some other patterns when approaching the microscopic scales. Therefore, a straight line in the $\ln N(\varepsilon)$ vs. $\ln(l/\varepsilon)$ diagram can be observed in a range of ε only (Figure 3). This range must extend over *several decades* in order to imply the existence of a fractal structure.

4. Fractals are *selfsimilar* objects, i.e. they look the same on many different scales in the range where (2) holds. This is consistent with the fact that a scaling form

$$N(\lambda\varepsilon) = \lambda^{-D_0} N(\varepsilon), \tag{3}$$

where λ is an arbitrary positive number, follows from (2). Among usual geometrical objects there are also selfsimilar ones (e.g. line, plane) but they are simple. Fractals are, thus, *nontrivial* selfsimilar objects.

The fractal dimension turned out to be a very good characteristic of different structures in nature [2]. Moreover, in certain cases D_0 proved to be universal, i.e. the same for a class of systems. In many cases (coast line: $D_0 \cong 1.25$, landscape: $D_0 \cong 2.2$) the origin of this universality is not yet known, in other cases, however, (*polymer* coil: $D_0 \cong 1.66$, the region of active, nonlaminar flow in fully developed *turbulence*: $D_0 \cong 2.8-3.0$) the physical reasons of the universality seem to be understood [2].

The aim of this report is to give a *tutorial introduction* to help new-comers from different fields of science to learn recent notions and concepts related to fractals. For this reason, mainly mathematical examples with simple *recurrent* structures will be used which are best suited for clarifying concepts like multifractality or thermodynamical formalism. Nevertheless, the general results and relations we obtain hold for all fractal objects. The article is not intended to be a historical survey or a complete review of the field, as reflected also in the choice of references which are concentrated only on a few phenomena mentioned in the paper. Even these selections are necessarily incomplete, but the author hopes they are sufficient to help the reader in further orientation.

3. Thin Fractals – Fat Fractals

If the fractal dimension D_0 of a set is smaller than the Euclidean dimension d, the observed volume

$$V(l) = N(\varepsilon)\, l^d \sim L^{D_0}\, l^{d-D_0} \tag{4}$$

depends, actually, on the grid size l in the range where (2) holds. Such system are, therefore, fractals. We call them *thin* fractals since $V(l)$ would vanish in the limit $l \to 0$. Such fractals are, in a mathematical sense, objects of measure zero in the d-dimensional space.

It is worth mentioning that $D_0 = d$ does not necessarily imply that the object is a usual body. In several cases a power law behaviour

$$V(l) - V(0) \sim L^{d-\gamma}\, l^{\gamma} \tag{5}$$

has been found [2, 11, 12], where $\gamma > 0$ is a new exponent (not a dimension!) and $V(0)$ is the finite limiting value of the observed volume obtained for $l \to 0$. Such objects are also fractals. These fractals are called *fat* [11] since their d-dimensional volume is nonzero.

A simple analytically tractable example is obtained by modifying the construction of the triadic Cantor set in such a way [11] that, at the n-th stage, the fraction of each interval removed is $(1/3)^n$, rather than $1/3$ (e.g. at the second stage the middle ninth of each interval is removed).

Fat fractals are also common in nature. Examples include [2] the vascular system, the branching structure of bronchia in the lung, river networks, and the top of certain trees which are with a very good accuracy space filling objects.

In what follows we shall mainly deal with thin fractals.

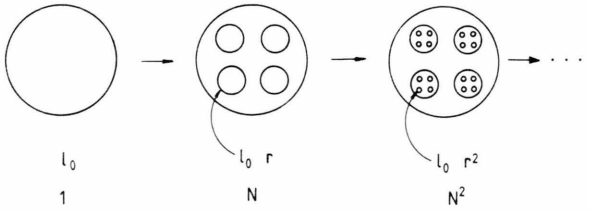

Fig. 4. Schematic construction of a one-scale fractal.

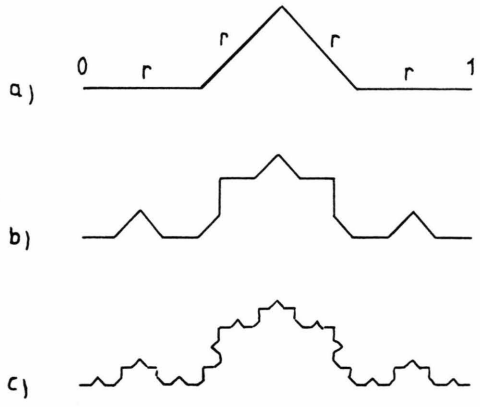

Fig. 5. The first steps in constructing a Koch curve ($r = 0.3$). The fractal dimension of the resulting fractal is $D_0 = \ln 4/\ln(1/0.3) = 1.151$.

4. Deterministic Fractals

We study a few classes of fractals which are constructed by *deterministic* rules. First, exactly selfsimilar objects possessing a recursive structure will be considered.

One-Scale Fractals

The rule of construction for such fractals can be schematically represented as on Figure 4. One starts with a single object of linear size l_0. In the next step this object is divided into N identical pieces each of which is a reduced version of the original object by the *same* factor $r < 1$ (hence the name *one*-scale fractal). The procedure is then repeated in the next step so that N of the newly created pieces of size $l_0 r^2$ are arranged inside a piece of size $l_0 r$ exactly in the same way as these parts are arranged inside the original object (Fig. 4). The fractal is then obtained by applying this rule subsequently ad infinitum.

Consequently, the fractal can be divided into N identical parts, each being rescaled versions, by a factor r, of the complete set. Let $N_1(\varepsilon)$ denote the number of boxes on a grid of size $l \ll L$ (L is the diameter of the fractal) needed to cover one such part. Then the number of boxes needed to cover the complete fractal is

$$N(\varepsilon) = NN_1(\varepsilon) . \tag{6}$$

Due to the similarity, $N_1(\varepsilon)$ is the same as the number of boxes needed to cover the complete set with boxes of size l/r:

$$N_1(\varepsilon) = N(\varepsilon/r) . \tag{7}$$

By putting (6), (7), and (2) together,

$$D_0 = \frac{\ln N}{\ln(1/r)} \tag{8}$$

is obtained, which is an exact result for one-scale fractals [2].

Example I: Koch's Curve

The construction of a Koch curve [13, 2] proceeds as follows. Let us cut out from the unit interval the interval $(r, 1-r)$, where $1/4 \leqq r \leqq 1/2$ is a parameter. To the two newly created endpoints a V-shaped curve is added, both sides of which are straight and of length r, as shown on Fig. 5a. The same process is repeated with all sides of length r, and then again and again (Fig. 5b, c) ad infinitum.

By comparing this rule with the general scheme we find $N = 4$. The fractal dimension of a Koch curve is therefore $D_0 = \ln 4/\ln(1/r)$. It is worth noting that the length of this curve (the analogue of the surface area) diverges with the resolution: the length measured by bars of length r^m, $m > 1$ fixed, is 4^m, as follows from the construction.

Example II: Snowflake Fractal

The construction rule [14] shown in Fig. 6 can be considered as a model for aggregation processes. The "seed" configuration ($n = 0$) is a symmetric cross built by five particles. The configuration at the n-th stage is obtained by adding to the four corners of the $(n-1)$-th stage configuration the cluster corresponding to the $(n-1)$-th stage of the growth. By reducing the n-th stage configuration by a factor 3^n one finds a series of objects of the same linear size [14]. The rule of con-

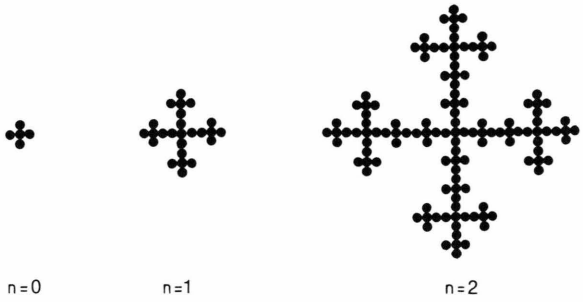

Fig. 6. The first steps in constructing a snowflake fractal with a growth process.

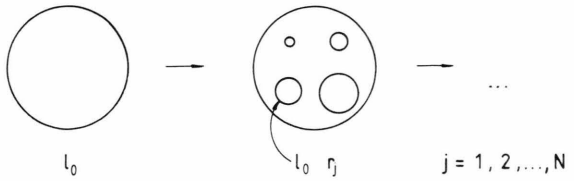

Fig. 7. Schematic construction of a multi-scale fractal.

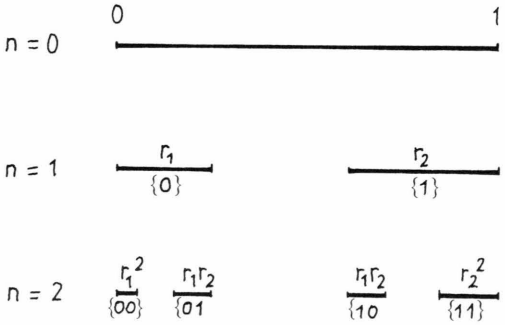

Fig. 8. The first steps in constructing a two-scale Cantor set ($r_1 = 0.25$, $r_2 = 0.4$). For the resulting fractal $D_0 = 0.611$. The codes associated with the intervals will be explained in Section 14.

struction corresponds then to that represented in Fig. 4 with parameters $N = 5$, $r = 1/3$. Consequently, the dimension of the fractal is $D_0 = \ln 5/\ln 3 = 1.465$.

Multi-Scale Fractals

The essential difference between the construction of multi-scale and one-scale fractals is the fact that the starting object is now divided into N parts which are *not* all identical. However, all of these are reduced versions of the original object by certain factors $r_j < 1$, $j = 1, \ldots, N$ (all r_j cannot be identical) [2, 15]. The procedure is then repeated in a similar way ad infinitum (Figure 7). Consequently, the resulting fractal can be divided into N parts, each being rescaled versions of the complete fractal. Let $N_j(\varepsilon)$ denote the number of boxes on a grid (size $l \ll L$) needed to cover the j-th such part. The number of boxes needed to cover the complete fractal is

$$N(\varepsilon) = \sum_{j=1}^{N} N_j(\varepsilon) . \tag{9}$$

From the similarity property,

$$N_j(\varepsilon) = N(\varepsilon/r_j) \tag{10}$$

follows. These relations and (2) then yield [2, 3]

$$\sum_{j=1}^{N} r_j^{D_0} = 1 \tag{11}$$

which is an exact (implicit) equation for the dimension of multi-scale fractals. For $r_1 = \ldots = r_N \equiv r$ result (8) is, of course, recovered.

Example III: Two-Scale Cantor Set

This fractal is obtained by dividing the interval [0, 1] as shown in Fig. 8 [16]. We initially replace the unit interval with two intervals of length r_1 and r_2 ($r_1 + r_2 < 1$). At the next stage of the construction the same process is applied to each of these two intervals. The procedure is then repeated again and again. The general formula (11) yields for the dimension

$$r_1^{D_0} + r_2^{D_0} = 1 . \tag{12}$$

(The one-scale Cantor set is obtained as the limiting case $r_1 = r_2 = r$. Then $D_0 = \ln 2/\ln(1/r)$. For the triadic Cantor set $r = 1/3$ and $D_0 = 0.631$.)

Example IV: Two-Scale Snowflake Fractal

This is a generalization [17] of Example II. The "seed" configuration is now a single particle. The configuration at the n-th stage is obtained by adding the twice enlarged version of the cluster corresponding to the $(n-1)$-th stage of the growth to the four corners of the $(n-1)$-th stage configuration (Figure 9). Reducing the object obtained after n steps by a factor 5^n the general scheme (Fig. 7) can be applied. Since $r_1 = 1/5$, $r_2 = \ldots = r_5 = 2/5$ we find

$$5^{-D_0} + 4\,(5/2)^{-D_0} = 1 \tag{13}$$

as an equation for D_0. Its solution is $D_0 = 1.601$.

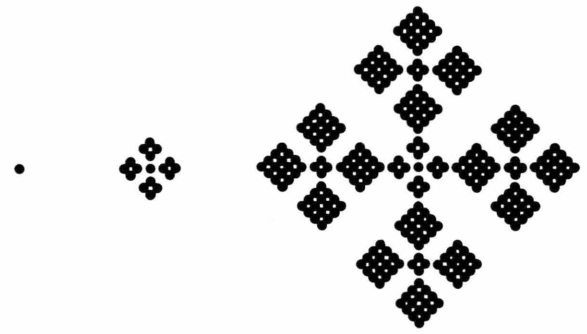

Fig. 9. The first steps in constructing a two-scale snowflake fractal by means of a growth process.

5. Fractal functions*

There exist continuous *functions* given by simple formulae, which are nowhere differentiable. The graph of such a function turns out to be a fractal curve. These fractals are also deterministic ones.

We consider, first, the Fourier series

$$C(t) \equiv \sum_{n=-\infty}^{\infty} \frac{1-\cos(\gamma^n t)}{\gamma^{(2-D)n}}, \tag{14}$$

the so-called Weierstrass-Mandelbrot function [2, 18]. In the range of parameters

$$1 < D < 2, \quad \gamma > 1, \tag{15}$$

$C(t)$ is continuous but the series defining $\mathrm{d}C(t)/\mathrm{d}t$ diverges everywhere.

By a formal replacement $n \to n+1$ the scaling relation

$$C(\gamma t) = \gamma^{2-D} C(t) \tag{16}$$

follows from (14) with $\gamma > 0$. Consequently, the graph of $C(t)$ on the interval $t_0 \leqq t \leqq \gamma t_0$, t_0 arbitrary, can be obtained by magnifying the graph in the range $t_0/\gamma \leqq t \leqq t_0$ with factors γ and γ^{2-D} in horizontal and vertical directions, respectively. This nontrivial symmetry, the so-called *self-affinity* [2, 19], can clearly be observed in Figure 10. The fractal dimension** of the graph of $C(t)$ has been shown [18] to be

$$D_0 = D \tag{17}$$

in the parameter range (15). As a further consequence of (16) the curve $C(t)$ possesses *no scale at all*, which is also demonstrated on Figure 10.

The first example, of great historical importance, for a continuous but nowhere differentiable function was given by Weierstrass [20]. It is defined as

$$W(t) = \sum_{n=0}^{\infty} \frac{\cos(\gamma^n t)}{\gamma^{(2-D)n}}. \tag{18}$$

This function is more complicated than $C(t)$ since a scaling relation holds now only up to an additive smooth function. For $n \geqq 0$ in (18),

$$W(\gamma t) = \gamma^{2-D} W(t) + \cos(t). \tag{19}$$

Consequently, the graph of $W(t)$ does have a largest scale, $W(t)$ has a maximum (Figure 11).

For the local fractal dimension of the graph, (17) has been shown to hold [21] in the parameter range given by (15).

6. Random Fractals

Fractals which are generated by nondeterministic rules are called *random*. In order to illustrate the difference between the construction of deterministic and random fractals, let us consider the following example. In the first step of the deterministic construction the upper right quarter of a square is cut out. Then the same procedure is repeated in all remaining squares (Figure 12a). Modifying this rule by choosing stochastically which of the four quarters of the square in question is deleted, a random fractal is obtained (Figure 12b). Although the geometrical appearance of these two sets is quite different, their fractal dimensions coincide since the number of boxes needed to cover them is the same.

There exist also random fractal functions. The most extensively studied phenomenon connected with them is *diffusion* or *Brownian motion*. The displacement $x(t)$ of a Brownian particle moving along a line is a stochastic variable with zero average and with variance

$$\langle x^2(t) \rangle \sim t, \tag{20}$$

where the bracket denotes averaging over several realizations. Relation (20), implies usual diffusion. The

* Sections 5, 6 provide an outlook on certain important fields of fractals but can be omitted when reading the paper as an introduction to the subject of multifractals.

** For self-affine sets a nontrivial fractal dimension, called the *local* dimension, can be obtained only by using a very fine grid. On long scales, (2) yields a trivial integer value (in our case unity) for D_0 [19, 9].

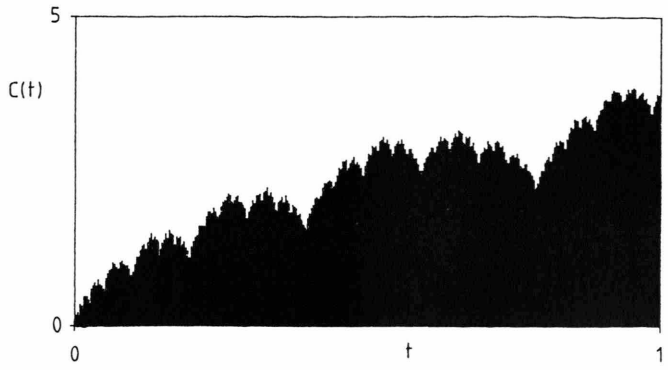

Fig. 10. The Weierstrass-Mandelbrot function for $D = 1.5$, $\gamma = 2$. The plot was obtained by keeping Fourier components with $|n| \leqq 10$ in (14).

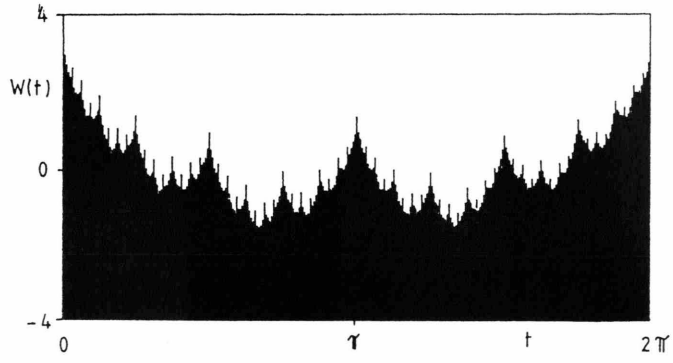

Fig. 11. The Weierstrass function for $D = 1.5$, $\gamma = 2$ when it is 2π-periodic. The plot was obtained by keeping Fourier components with $n \leqq 10$ in (18). Note that the fractal dimensions of the curves shown on Figs. 10 and 11 are the same.

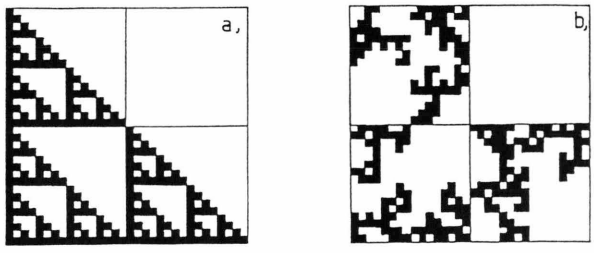

Fig. 12. Deterministic fractal (a) and a random version (b) of it. The objects are exhibited here as obtained after five steps of construction. The fractal dimension is for both cases $D_0 = \ln 3/\ln 2 = 1.585$.

graph of $x(t)$ was proved [2, 22] to be a fractal curve with local fractal dimension $D_0 = 1.5$ (Figure 13b).

The *fractional* Brownian motion [2, 22] is an extension of the concept of the usual Brownian motion. The displacement $x(t)$ of a particle following such a motion in one dimension is – by definition – a stochastic variable with zero average and with variance

$$\langle x^2(t) \rangle \sim t^{2H}, \tag{21}$$

where $0 < H < 1$. For $H \neq 1/2$ this corresponds to an anomalous diffusion with correlated increments. Such correlations extend to arbitrarily long time scales and have a large effect on the visual appearance of the traces (Figure 13). The graphs are self-affine fractal curves with a local fractal dimension [2, 22]

$$D_0 = 2 - H. \tag{22}$$

Fractional Brownian motion is used when making computer simulations of fractals like mountainous terrains or clouds [2, 22].

Fractals in nature are typically random ones. The field of applications in physics is also extremely broad and ranges from *percolation* [23] and *pattern formation* through growth processes [4, 5, 24, 25] to *chaos* [26] and *turbulence* [2, 27, 28].

Despite this great practical relevance we shall, in what follows, mainly be interested in deterministic fractals which are best suited for an elementary introduction of further new concepts.

7. Fractal Dimension for Composite Fractals

Several fractals proved to be composite, i.e. to be unions of fractal subsets. Let us assume that a com-

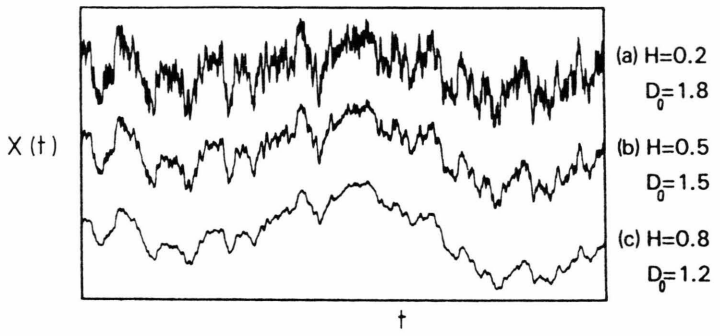

Fig. 13. Traces of fractional Brownian motion at three different values of the parameter H (after [22]).

plete set of linear size L consists of m fractal subsets, and let $N_k(\varepsilon)$, $\varepsilon = l/L$, denote the number of boxes of size l needed to cover the k-th subset on a grid. For small box size $N_k(\varepsilon) \sim \varepsilon^{-D_0^{(k)}}$, where $D_0^{(k)}$ is the fractal dimension of the subset. Since the overlap among different covers vanishes with decreasing box size, the number of boxes needed to cover the complete set is

$$N(\varepsilon) = \sum_{k=1}^{m} N_k(\varepsilon) . \tag{23}$$

On the right hand side the contribution with the largest $D_0^{(k)}$ dominates for $\varepsilon \to 0$, thus, from (2)

$$D_0 = \max D_0^{(k)} . \tag{24}$$

The fractal dimension of the complete set is the same as the largest dimension of the subsets.

This relation tells us that simple and complete fractals *cannot* be distinguished by measuring the fractal dimension alone. Consequently, a more detailled description of fractals requires the introduction of further parameters characterizing different subfractals. How this can be done will be discussed in the next sections.

II. Multifractals

8. Fractal Measures

In several phenomena fractals appear not only as strange geometrical objects but provide stages on which "something is going on". Physical processes on fractals may generate *stationary distributions* (measures). Fractals with time independent distribution on them are called *fractal measures* (for a quantitative definition see the end of Section 11). The quantity which may be distributed on a given fractal depends on the physical system in question. Here we mention only a few examples. On random resistor networks [29] the *voltage* or current distribution can be measured. For aggregation processes the probability that a given site is the next to grow, the so-called *growth probability*, gives a distribution [30, 31]. In the case of fully developed turbulence the *velocity difference* inside eddies is a quantity defining a measure [27, 28]. It is to be noted that different distributions may exist on a fractal leading to the existence of different fractal measures on the same support.

It is a recent observation [27, 32, 30, 16] that nontrivial distributions can be considered as analysers of strange sets. They open up *different fractal subsets* by e.g. selecting subsets giving the dominating contributions to different moments of the distributions. If this is the case, the system will be called *multifractal* [32, 30, 16, 33]. Different distributions may lead to different multifractal properties. It may happen that a fractal with a given measure is a multifractal but with another one it is not.

The following simple example illustrates how a nontrivial distribution selects different fractal subsets of its support.

9. An Example for Multifractals

We consider here a probability distribution on the unit interval constructed by a simple rule [34]. In the first step the middle third of the interval is made more (or less) probable than the outer thirds. Let the probability of each of these pieces be p_1, and the probability of the middle third be $p_2 = 1 - 2p_1$ (Figure 14a). In the next step each piece is divided again into thirds, and the probability is redistributed whithin each of

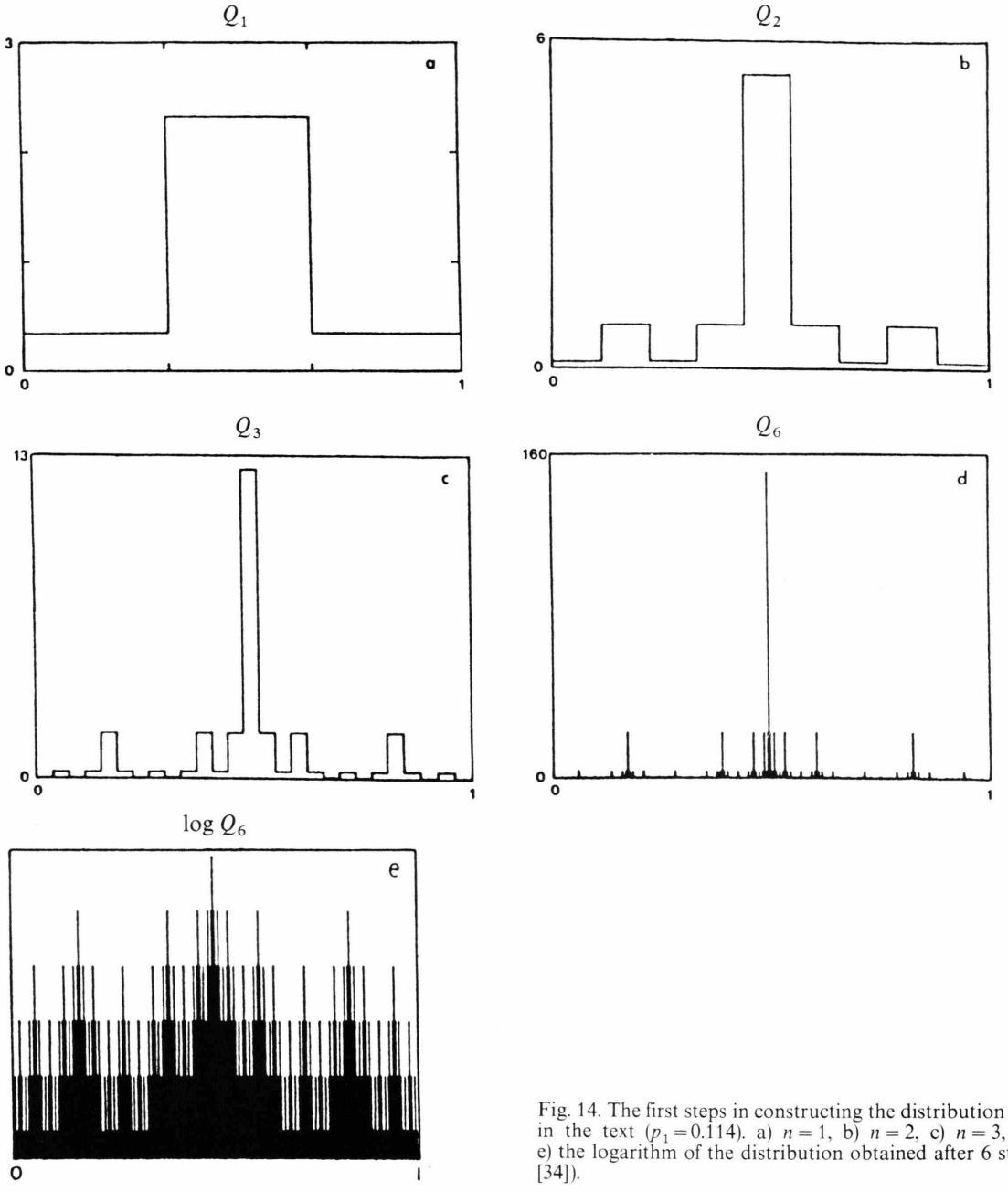

Fig. 14. The first steps in constructing the distribution described in the text ($p_1 = 0.114$). a) $n = 1$, b) $n = 2$, c) $n = 3$, d) $n = 6$, e) the logarithm of the distribution obtained after 6 steps (after [34]).

these nine pieces so that the ratios within each third are the same as those of the first stage distribution (Figure 14 b). The procedure is repeated again and again (Figure 14 c, d). The distribution becomes so inhomogeneous that its internal regular structure can be seen only on a logarithmic scale (Figure 14 e). The density of the asymptotic distribution obtained after an infinite number of steps is then discontinuous everywhere.

When studying the properties of this distribution one has to use a grid of finite size. Now not only the number of boxes is important but also the measures inside boxes, the so-called *box probabilities*. Let us take a grid obtained by subdividing the unit intervals

into intervals (boxes) of size $l = \varepsilon = (1/3)^n$ with $n \gg 1$. It follows from the construction described above that the box probabilities can take on one of the values

$$P_m = p_1^m p_2^{n-m}, \tag{25}$$

where m is an integer between 0 and n. Since the number of boxes $3^n \gg n$, there must be a degeneracy in the distribution:

$$N_m = \binom{n}{m} 2^m \tag{26}$$

is the number of boxes with the same measure P_m. For the sake of definitness we assume $p_2 > p_1$.

First, we ask which boxes give the main contribution to the total probability when refining the grid. Although the most probable box is that in the middle, with content $P_0 = p_2^n$, it is alone. Its contribution is negligible for $n \to \infty$ since $p_2 < 1$. The most rarified boxes ($P_n = p_1^n$) are numerous, nevertheless the probability in such boxes is also negligible since $(2p_1)^n \to 0$. It is, therefore, plausible that, for large n, columns very close to some medium hight give the main contribution. More precisely, for $n \to \infty$ there exists a single index $m = m_1(n)$ between 0 and n, so that only boxes with P_{m_1} contribute to the total probability: $N_{m_1} P_{m_1} \to 1$. Consequently, none of the other boxes are important from the point of view of the total measure. An easy calculation (see Appendix) yields

$$m_1/n = 2p_1 \tag{27}$$

(note that m/n is a quasi continuous quantity for $n \gg 1$).

The number N_{m_1} of the relevant boxes increases, of course, exponentially with n. Since the resolution is $\varepsilon = (1/3)^n$, N_{m_1} can be written as

$$N_{m_1} = \varepsilon^{-f_1}, \tag{28}$$

i.e. these boxes cover a fractal *subset* of the unit interval, and f_1 is the *dimension* of this subset. From (26)–(28)

$$f_1 = \frac{2p_1 \ln p_1 + p_2 \ln p_2}{\ln 1/3} \tag{29}$$

is obtained.

Next, we investigate the q-th power of the box probabilities, where $-\infty < q < \infty$ is a parameter. The total amount of these quantities is $\sum_{\mathrm{m}} N_m P_m^q = (2p_1^q + p_2^q)^n$. Similarly to the previous case, columns of a certain height contribute only to this sum. At a fixed q, boxes with P_{m_q} are found to dominate, where

$$\frac{m_q}{n} = \frac{2p_1^q}{2p_1^q + p_2^q}. \tag{30}$$

Their number increases again exponentially with n. We can, therefore, write

$$N_{m_q} = \varepsilon^{-f_q}. \tag{31}$$

This means that *a subset of fractal dimension f_q gives the dominant contribution to the sum of the q-th power of the box probablities*. Note that for $q \neq 1$ this subset is different from that contributing to the total measure. In our example

$$f_q = \left[\frac{2p_1^q \ln p_1^q + p_2^q \ln p_2^q}{2p_1^q + p_2^q} - \ln(2p_1^q + p_2^q) \right] \frac{1}{\ln(1/3)} \tag{32}$$

is obtained as can be checked easily.

By increasing (decreasing) the exponent q, boxes with higher (lower) probabilities, i.e. fractal regions with denser (more rarified) occupation are selected. In fact, the limit $q \to \infty$ picks up the most probable box which is alone. Consequently, $f_\infty = 0$. The opposite limit selects the least probable boxes. Their number is 2^n, therefore $f_{-\infty} = \ln 2/\ln 3$. These limiting results can be obtained also from (32).

We have, thus, demonstrated that the contribution of the sum of different powers of the box probabilities is dominated by different fractal subsets. The *spectrum* f_q of their fractal dimension provides a *characteristic* of this *multifractal*. The example also illustrates that an *inhomogeneous* distribution on a *non-fractal* support (here the unit interval) can be multifractal.

In addition to the fractal dimension also the content of those boxes which contribute, i.e. the probability P_{m_q} belonging to each of them, is an important quantity. Since, however, P_{m_q} depends on n (or ε), it is better to introduce an ε-independent parameter, the *crowding index* α_q, by writing

$$P_{m_q} = \varepsilon^{\alpha_q}. \tag{33}$$

From (25) and (30)

$$\alpha_q = \frac{2p_1^q \ln p_1 + p_2^q \ln p_2}{2p_1^q + p_2^q} \frac{1}{\ln(1/3)} \tag{34}$$

is found. The values of α_q lie in the range between $\alpha_\infty = \ln p_2/\ln(1/3)$ and $\alpha_{-\infty} = \ln p_1/\ln(1/3)$. (For the particular choice of p_1 used in constructing Figs. 14–17 ($p_1 = 0.114$) we obtain $\alpha_\infty = 0.234$ and $\alpha_{-\infty} = 1.981$.)

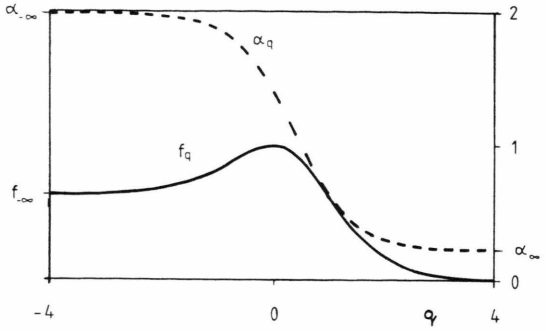

Fig. 15. The q-dependence of the fractal dimension f_q, (32), and of the crowding index α_q, (34), for the multifractal constructed in the previous Figure.

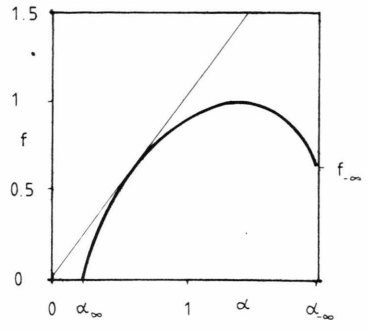

Fig. 16. The $f(\alpha)$ spectrum for the multifractal of Sect. 9 as obtained from (32) and (34) by eliminating q. The straight line is the diagonal $f=\alpha$.

The spectra f_q and α_q are exhibited in Fig. 15 for a case $p_2 > p_1$. Note that the multifractal properties are lost for the parameter values $p_1 = p_2 = 1/3$ when $f_q = \alpha_q = 1$, since the density is then constant over the whole interval. A similar case is obtained for $p_2 = 0$, $p_1 = 1/2$ when $f_q = \alpha_q = \ln 2/\ln 3$. This corresponds to the familiar triadic Cantor set with a *uniform* distribution on it.

10. Characterization of General Multifractals

In order to describe multifractal properties a uniform grid of size l, as introduced in Section 1, is used again. Let P_i denote the measure or probability inside the i-th box: for empty boxes P_i vanishes. A central quantity [35, 15, 36] is

$$\chi_q(l, L) \equiv \sum_i P_i^q , \tag{35}$$

the sum over all boxes of the q-th power of the box probabilities, $-\infty < q < \infty$. χ_q depends only on the dimensionless number $\varepsilon \equiv l/L$, where L is the linear size of the support: $\chi_q(l, L) \equiv \chi_q(\varepsilon)$. For $q = 0$, (35) yields the number of boxes needed to cover the support. Since the distribution should be normalized, $\chi_1(\varepsilon) \equiv 1$ holds.

The properties of the previous example turn out to be typical for multifractals. For $\varepsilon \to 0$ the contribution to $\chi_q(\varepsilon)$ with a given q comes from a subset of all possible boxes. These boxes cover a fractal, i.e. their number $N_q(\varepsilon)$ depends on ε as

$$N_q(\varepsilon) \sim \varepsilon^{-f_q} , \tag{36}$$

where f_q is the fractal dimension of the *subset*. Furthermore, the content of each contributing box is approximately a constant, P_q. The crowding index α_q for these boxes is defined by the asymptotic relation

$$P_q \sim \varepsilon^{\alpha_q} . \tag{37}$$

A multifractal is then characterized by the spectra f_q and α_q.

Since $\chi_0(\varepsilon) = N(\varepsilon)$, the quantity f_0 is the fractal dimension D_0 of the support. It follows from the property of composite fractals (Section 7) that $f_0 > f_q$ for $q \neq 0$ since the multifractal is the union of all subfractals with dimension f_q. The function f_q vs. q increases until it reaches its maximum D_0 and then decreases. As higher powers select denser regions, α_q is monotonously decreasing (see Figure 15).

A simple fractal corresponds in this picture to the special case $f_q = \alpha_q \equiv D_0$.

The elimination of the variable q between f_q and α_q leads to a new characteristic, to the so-called $f(\alpha)$ *spectrum* [16]. Direct definitions of α and $f(\alpha)$ can be given as follows. For $\varepsilon \to 0$ around each point of the fractal one finds

$$P_i \sim \varepsilon^{\alpha} , \tag{38}$$

where α is position dependent. Relation (38) defines the set of *crowding indices* [16] (or Hölder exponents [2]) α. At any fixed ε there exist, however, several boxes with a given crowding index, say, α. Their number $N_\alpha(\varepsilon)$ increases with ε like

$$N_\alpha(\varepsilon) \sim \varepsilon^{-f(\alpha)} , \tag{39}$$

i.e. these boxes cover a subset of fractal dimension $f(\alpha)$. The variable α may take on values from a range $[\alpha_\infty, \alpha_{-\infty}]$, and $f(\alpha)$ turns out to be, in general, a single humped function with D_0 as its maximum [16] (Figure 16). The $f(\alpha)$ spectrum of a simple fractal consists of a single point.

Before turning to the question how α_q and f_q can be obtained from $f(\alpha)$ it is worth introducing the concept of generalized dimensions.

11. Generalized Dimensions

The quantity $\chi_q(\varepsilon)$ is found to follow a power law behaviour as $\varepsilon \to 0$:

$$\chi_q(\varepsilon) \sim \varepsilon^{(q-1)D_q}, \tag{40}$$

where D_q is the so-called *order q generalized dimension* [35, 27, 15, 36]. The factor $(q-1)$ has been pulled out in the exponent to ensure automatically the relation $\chi_1(\varepsilon) \equiv 1$. Consequently, the D_q's are positive numbers. Their values monotonously decrease with q [15] (Figure 17). For simple fractals all the D_q's coincide.

It is easy now to connect the generalized dimensions and the spectra f_q, α_q. Since the contribution to $\chi_q(\varepsilon)$ is given by boxes with content P_q we have $\chi_q(\varepsilon) = N_q(\varepsilon) P_q^q$. This implies via (36), (37) and (40)

$$(q-1) D_q = q \alpha_q - f_q . \tag{41}$$

For $q = 0$ the relation $D_0 = f_0$ is recovered. Furthermore, as f_q is finite, $D_{\pm\infty} = \alpha_{\pm\infty}$ follows.

In order to find the relation to the $f(\alpha)$ spectrum let us notice that $\chi_q(\varepsilon)$ can be written (see (35), (38), (39)) for $\varepsilon \to 0$ as

$$\chi_q(\varepsilon) \sim \int \varepsilon^{q\alpha - f(\alpha)} \, \mathrm{d}\alpha , \tag{42}$$

when α is a quasi continuous variable. Since ε is very small, the integral will be dominated by the value of α which makes the exponent *minimal*. This immediately leads to (41) with the conditions

$$\left.\frac{\mathrm{d}f(\alpha)}{\mathrm{d}\alpha}\right|_{\alpha_q} = q ; \quad f_q = f(\alpha_q) . \tag{43}$$

α_q is, therefore, that particular value of the crowding index for which the derivative of $f(\alpha)$ is exactly q. As a consequence, also the spectra $f(\alpha)$ and $(1-q) D_q$ are connected: they are Legendre transforms of each other (see (41)).

The case of the order 1 generalized dimension is of special importance. From (41) and its derivative taken at $q = 1$ we find

$$D_1 = \alpha_1 = f_1 . \tag{44}$$

This relation together with (43) explains why the f_q and α_q curves touch each other at $q = 1$ (Fig. 15) and why $f(\alpha)$ is tangent to the diagonal exactly at a point where $f(\alpha) = \alpha = D_1$ (Figure 16). Furthermore, by performing the limit $q \to 1$ in (35) and (40) one obtains

$$-\sum_i P_i \ln P_i \sim D_1 \ln(1/\varepsilon) . \tag{45}$$

The quantity D_1 thus measures how the information (left hand side) scales with $\ln(1/\varepsilon)$. Therefore D_1 has been called the *information* dimension [37, 34]. Moreover, this concept has been used to give a precise definition of fractal measures [34]: a distribution is said to be a fractal measure if its fractal dimension exceeds its information dimension. In this sense the example of Sect. 9 is a fractal measure and, moreover, all fractal measures are multifractals. (The value of p_1 used in Fig. 14 was chosen in such a way that $D_1 = \ln 2 / \ln 3$, i.e. the same as the fractal dimension of the triadic Cantor set. The fractal dimension of the support is, of course, unity in this example.)

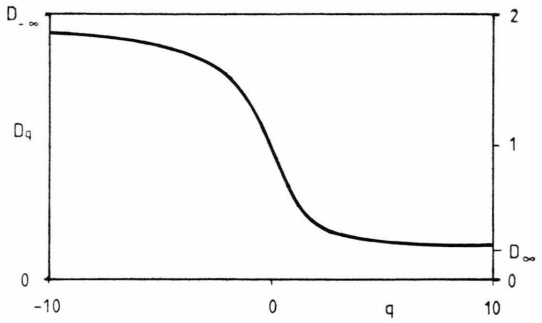

Fig. 17. The D_q spectrum for the multifractal of Section 9.

It is worth noting that despite their name, the generalized dimensions D_q $(q \neq 0, 1)$ are not dimensions. as expressed by (41). This can also be seen from the fact that all D_q with a negative q are in the example of Sect. 9 larger than 1 (Fig. 17). Nevertheless, the spectra D_q and $f(\alpha)$ (or f_q and α_q) provide *equivalent* characterizations of multifractals. (For another interpretation of D_q see [27].)

Finally, we mention that distributions on fat fractals can also be multifractals characterized not only by D_q but by another set of exponents γ_q obtained by generalizing (5) [38].

12. Fractals Measures with an Exact Recursive Structure

The class of fractal measures possessing an exact recursive structure provides analytically tractable

cases. We consider measures for which the rule of construction is based on that of multi-scale fractals (Section 4, Fig. 7). Now the *redistribution* of the *measure* is also to be defined. Let p_j be the probability associated with the j-th piece which is the reduced version of the original one by a factor r_j, $\sum_{j=1}^{N} p_j = 1$. At the next stage of construction each piece is further divided into N pieces, each with a probability reduced by a factor p_j and size by a factor r_j, etc. The support of the resulting measure can, therefore, be divided into N parts, each being a rescaled version of the complete support, by a factor r_j. Each such part carries an amount p_j of the total measure. From this similarity property

$$\chi_{q,j}(\varepsilon) = p_j^q \chi_q(\varepsilon/r_j) \tag{46}$$

follows, where $\chi_{q,j}(\varepsilon)$ stands for the quantity defined by (35), evaluated for the j-th piece by using a grid of size l ($\varepsilon = l/L$, L is the linear size of the support). For the complete system

$$\chi_q(\varepsilon) = \sum_{j=1}^{N} \chi_{q,j}(\varepsilon) . \tag{47}$$

From these relations and from (40)

$$\sum_{j=1}^{N} \frac{p_j^q}{r_j^{(q-1)D_q}} = 1 \tag{48}$$

is obtained, which is an exact equation for the generalized dimension D_q [15]. For $q = 0$, of course, (11) is recovered.

If the support is a one-scale object, i.e. if $r_j = r$ for all j, the implicite equation (48) can be solved, yielding

$$D_q = \frac{1}{q-1} \frac{\ln\left(\sum_{j=1}^{N} p_j^q\right)}{\ln r} . \tag{49}$$

This result applies also to the example of Sect. 9, where $N = 3$, $r = 1/3$ and $p_1 = p_3$.

Note that in cases when the probability is distributed uniformly on a one-scale support ($p_j = 1/N$), multifractal properties are lost since $D_q = \alpha_q = f_q = \ln N/\ln(1/r)$ for all q. For measures on multi-scale fractal supports, the property of multifractality is more persistent. Even a *uniform* distribution of the probability, i.e. the choice $p_j = r_j \Big/ \left(\sum_{j=1}^{N} r_j\right)$, leads to a nontrivial D_q spectrum, as can be seen from (48).

13. Geometrical Multifractality

Fractals on which a measure is distributed with a constant density form an interesting class, since in such cases multifractality, if present, manifests purely *geometrical* properties. The multifractal spectra can then be considered to characterize the fractal *support* itself. An example is provided by the two-scale Cantor set of Sect. 4 if the measure associated with an interval appearing in the construction (Fig. 8) is chosen to be proportional to the length of the interval (to the Lebesgue measure). Multifractal properties then reflect the heterogeneity in the size-distribution of these intervals.

Such *geometrical multifractality* [17] is of special importance for growing structures, where a distribution of constant density always exists and is of physical relevance. This is due to the fact that such systems are built up by identical particles and, therefore, the *mass* distribution on the growing structure is uniform. The multifractal properties with respect to this measure can be analysed along the lines described in Sect. 10 by chosing the box probability P_i to be proportional to the mass, or the number of particles, inside box i.

As an example, let us consider the two-scale snowflake fractal of Section 4. By reducing the object obtained after n steps of construction by a factor 5^n the general scheme worked out in the previous Section can be applied. The cluster consists of a smaller central and four larger pieces each having the overall shape of a square (Figure 9). Since the masses of these different sqaures are 1/17 and 4/17 parts of the total mass, one obtains [17] from (48)

$$(\tfrac{1}{17})^q \, 5^{(q-1)D_q} + 4\,(\tfrac{4}{17})^q \,(\tfrac{5}{2})^{(q-1)D_q} = 1. \tag{50}$$

The D_q values lie in the range between $D_\infty = \ln(17/4)/\ln(5/2) = 1.579$ and $D_{-\infty} = \ln 17/\ln 5 = 1.760$. The numbers appearing in (50) are linear size and area ratios of the five main squares, with respect to the data of the whole cluster, which reflects the fact that the multifractality is in this case of geometrical origin.

It is worth mentioning that a growing structure may be a multifractal, say, with respect to the growth probability and, simultaneously, a geometrical multifractal, i.e. a multifractal, with respect to the homogeneous mass distribution on the structure. The spectra for these two multifractals are then, of course, different.

In the next sections we introduce the so-called *thermodynamical formalism,* the importance of which in natural sciences has been realised only very recently. Besides providing a broad theoretical framework, using the language of classical statistical mechanics, this method possesses also practical relevance since it yields more accurate results than a direct application of the definitions of Chapts. I and II. The formalism is expected to become a widely used characterization of fractals and multifractals in the near future.

III. The Thermodynamical Formalism for Fractals and Multifractals

The thermodynamical formalism has been worked out in mathematics for describing fractal properties of chaotic dynamical systems [39]. It has recently been developed into a powerful technique [40–46], accessible also to experimentalists, providing more accurate results for the multifractal properties than box counting methods described in the previous sections. The concept of thermodynamical potentials has already been extended [47] for fractals which appear beyond the scope of dynamical systems. Based on these developments, we go here one step further and show how the thermodynamical formalism, built on an underlying *spin* system, can be worked out for such fractals. We shall see that the thermodynamical potentials arising in the formalism give the *most* general characterization of fractal and multifractal objects.

14. Encoding

Fractals are, in general, organized in a *hierarchical* way which is often reflected in their rules of construction. The fact that this hierarchy can be *encoded* is the basis for the thermodynamical formalism. To illustrate the concept of encoding, let us take again a simple example: the two-scale Cantor set of Sect. 4 (see Figure 8). The number of intervals used to approach the fractal doubles in each step, thus, at the n-th stage of construction there are 2^n intervals. Each of them can, therefore, be denoted by a binary number of length n. Let us apply the following rule: At the first stage the intervals of length r_1 and r_2 are associated with the symbols 0 and 1, respectively. In general, the last digit of the code for "daughter" intervals is 0 or 1 depending on whether their length were obtained by multiplying the length of their "mother" interval by r_1 or r_2 (Figure 8). Note that each code specifies an interval uniquely, but there is a *degeneracy* in the length of the intervals.

Several fractals can be encoded in a similar way. The encoding consists of two important items: i) the "ABC": the number k of independent symbols needed, and ii) the "grammar": the rules telling us which symbol sequences are allowed. In the previous example the grammar was trivial, all binary sequences occurred. In general, however, this is not the case and certain sequences are to be excluded. Such hierarchies can then be represented by a k-nary (binary, ternary, ...) *tree* which in the case of nontrivial grammars is not complete. Nevertheless, the number $W(n)$ of elements at the n-th level of the tree grows rapidly. For large n

$$W(n) \sim \exp(K_0 n), \tag{51}$$

where K_0 is an important characteristic, the *topological entropy* [26] of the hierarchy. On a k-nary tree $K_0 \leqq \ln k$, where the equality holds for a trivial grammar when the number of allowed sequences is just k^n.

Unfortunately, there is no general recipe for encoding a hierarchy. Only intuition and a detailed knowledge of the particular physical process might help to find the encoding of the fractal generated.

15. Statistical Analogy – Thermodynamical Potentials

In what follows we assume that the encoding has been found. Let $s_1 s_2 \ldots s_n \equiv \{s_i\} \equiv S_J$ denote a code occurring at the n-th stage of the hierarchy, where the elements s_i can take on values $0, 1, \ldots, k-1$, and $J = 1, \ldots, W(n)$ is a subscript specifying the code. To each code there is a box covering the part of the fractal which is associated with that particular code. In contrast to boxes of a uniform grid, these boxes fit to the fractal structure in a natural way providing an "optimal" coverage. For the sake of simplicity we assume that the boxes are d-dimensional *cubes* where d is the dimension of the space the fractal is embedded in. (An extension for more general cases can also be worked out.) The size of the cube associated with a code S_J is denoted by $l_J \equiv l(\{s_i\})$. Let $\varepsilon_J \equiv \varepsilon(\{s_i\}) = l_J/L$ represent the length scales measured in units of the diameter L of the fractal. It is worth introducing [41, 47] for a given code of length n the quantity

$$E_J \equiv E(\{s_i\}) = -\frac{1}{n} \ln \varepsilon_J . \tag{52}$$

In the limit $n \to \infty$ the value of E is positive and lies generally in an interval (E_-, E_+) [41, 47]. In other words, the characteristic exponents E tell us how rapidly the length scales decrease with increasing n. As n grows, there are, in the coverage, more and more boxes of the same size belonging to a given value of E. Their number $W(n, E)$ increases exponentially [41, 47], i.e. for large n we can write

$$W(n, E) \sim e^{S(E)n}. \tag{53}$$

The spectrum $S(E)$ characterizes the *length scale distribution* of the fractal. The maximal value of S is, of course, the topological entropy K_0 (Fig. 18 a). Illustrative examples will be given below.

Another characteristic can be obtained by considering the sum of the length scales raised to a power β. This sum changes with n also in an exponential fashion [41, 47], i.e. we have *

$$\sum_J \varepsilon_J^\beta \equiv \sum_{\{s_i\}} \varepsilon^\beta(\{s_i\}) \sim e^{-\beta F(\beta) n}, \tag{54}$$

where $-\infty < \beta < \infty$, and the sum is taken over all allowed sequences of length n ($n \gg 1$). We note by passing that $\exp\{-\beta F(\beta)\}$ appears also as an eigenvalue of an operator which can explicitly be constructed for fractals organized on a k-nary tree [46].

Two special values of $\beta F(\beta)$ follow immediately from (54). For $\beta = 0$ the sum is just the number of allowed sequences, thus

$$\beta F(\beta)|_{\beta=0} = -K_0. \tag{55}$$

Fractals are asymptotically selfsimilar: the coverage obtained at the n-th level is similar to that obtained at the $2n$-th level, for $n \gg 1$. The role of the similarity ratios defined in Sect. 4 (see Fig. 7) is then played just be the ε_J's. A comparison of (11) with $r_j = \varepsilon_j$, $N = W(n)$, and (54) shows that

$$\beta F(\beta)|_{\beta=D_0} = 0. \tag{56}$$

This means that the sum of the length scales raised to a power β remains finite in the $n \to \infty$ limit if β is chosen to be the fractal dimension. For fractals associated with dynamical systems relation (56) is the so-called Bowen-Ruelle formula obtained in [39]. (Strictly speaking, the particular β value for which $F(\beta)$ vanishes was proved to be the so-called Hausdorff dimension [2] which, however, coincides with D_0 disregarding very exotic examples.)

* The quantity $(-\beta F(\beta))$ is often called the pressure function [39]. We prefer to call $F(\beta)$ the free energy as follows from the statistical analogy (cf. table in the next column).

It is worth noting the parallelism between the present formalism and that of statistical mechanics. The key observation is that any allowed sequence $\{s_i\}$ can be associated with a *microstate* of a chain of n, in general interactive, spins (for $k = 2$ Ising model, otherwise k-state Potts model). Thus, the analogy can be summarized as follows:

Fractal characteristics	*Meaning in statistical mechanics*
code $\{s_i\}$	microstate
n	number of spins
$n \to \infty$	thermodynamic limit
β	inverse *temperature*
$\varepsilon_J^\beta = \exp(-\beta E_J n)$	Boltzmann factor
$\sum_J \varepsilon_J^\beta$	partition sum
E	*energy* per spin (in a macrostate)
W	number of microstates
S	*entropy* per spin
F	*free energy* per spin

Relations (53) and (54) correspond to a *microcanonical* and *canonical* description, respectively. In the thermodynamical limit these ensembles are equivalent, consequently, $\beta F(\beta)$ and $(-S(E))$ are Legendre transforms of each other, i.e.

$$F = E - \beta^{-1} S, \tag{57a}$$

where

$$dS/dE = \beta. \tag{57b}$$

They both decribe a *new* spectrum of fractal properties. $S(E)$ is typically a single humped function, while $\beta F(\beta)$ is monotonic increasing with a nonpositive second derivative (Figure 18).

The quantity $\beta F(\beta)$ is a linear function for one-scale fractals only. Using (51) and (54) $\beta F(\beta) = \beta E_0 - K_0$ is obtained, where E_0 is the energy value characterizing all the boxes.

In the example of the two-scale Cantor set, the length scales can be expressed as $\varepsilon(\{s_i\}) = r_1^m r_2^{n-m}$, where m is the number of 0's occurring in the (binary) code $\{s_i\}$. This number uniquely specifies, via (52), an exponent $E(m/n)$. Based on the fact that the multiplicity of intervals characterized by a given ratio m/n, or $E(m/n)$, is just $\binom{n}{m} = W(n, E)$, it is easy to check, using (53) and (54), that (58)

$$S(E) = -\frac{E - E_-}{\Delta E} \ln\left(\frac{E - E_-}{\Delta E}\right) - \frac{E_+ - E}{\Delta E} \ln\left(\frac{E_+ - E}{\Delta E}\right),$$

and

$$\beta F(\beta) = -\ln(e^{-\beta E_-} + e^{-\beta E_+}) \tag{59}$$

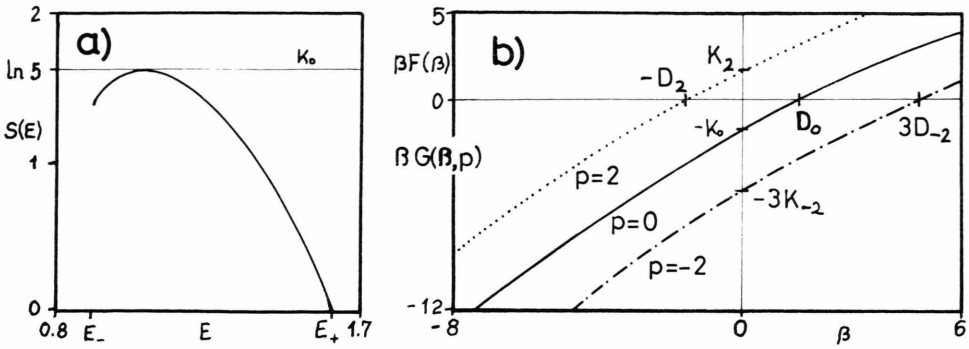

Fig. 18. Thermodynamical properties for the two-scale snowflake fractal (Fig. 9). – a) The plot of the entropy function $S(E) = -[(E-E_-)/\Delta E] \ln [(E-E_-)/\Delta E] - [(E_+-E)/\Delta E] \ln [(E_+-E)/(4\Delta E)]$, where $\Delta E = E_+ - E_-$ and $E_- = 0.916$, $E_+ = 1.609$. b) The plot of the free energy (heavy line) $\beta F(\beta) = -\ln(4(0.4)^\beta + (0.2)^\beta)$. For comparison also plots of the Gibbs potential (see Sect. 16) are shown. The latter is taken with respect to a measure defined with an exact recursive structure, as described in Sect. 12, on the two-scale snowflake fractal. Here the particular parameter values $p_1 = 0.12$, $p_2 = \ldots = p_5 = 0.22$ are chosen. Thus, $\beta G(\beta, p) = -\ln(4(0.22)^p (0.4)^\beta + (0.12)^p (0.2)^\beta)$. Dotted and dash-dotted lines correspond to $\beta G(\beta, p)$ at fixed "pressure" $p = 2$ and $p = -2$, respectively.

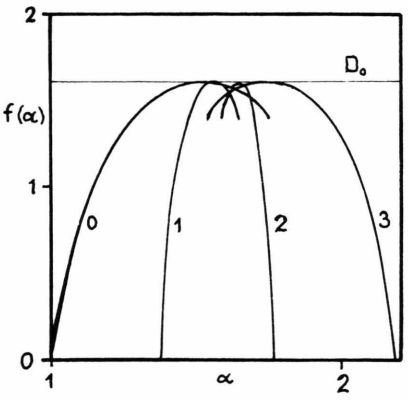

Fig. 19. $f(\alpha)$ spectra with respect to distributions (60) for the two-scale snowflake fractal. The values $\sigma = 0, 1, 2$ and 3 are taken and the spectrum is obtained via (63). The case $\sigma = 2$ corresponds to the D_q spectrum defined by (50). Note that for $\sigma = D_0$ measure (60) is not a multifractal since there exists then a single index $\alpha = D_0 = 1.601$ only (see (56), (61)). For $\sigma \to D_0$ the widths of the spectra tend to zero.

where $E_- = \ln(1/r_2)$, $E_+ = \ln(1/r_1)$ and $\Delta E = E_+ - E_-$. Here we have assumed, without loss of generality, that $r_2 > r_1$. These results show that the thermodynamical potentials of the two-scale Cantor set are those of n *noninteractive* two-state systems with energy levels E_-, E_+ (e.g. spins in magnetic field) [48].

The two-scale snowflake fractal (Fig. 9) might seem to be a less trivial example. In this case the "ABC" must have 5 elements, but the fractal still shares the thermodynamics with n independent spins. They are now 5-state spins, the lowest energy level of which is 4 times *degenerated* ($E_- = \ln(5/2) = 0.916$, $E_+ = \ln 5 = 1.609$). It is recommended that the reader derive the expressions for the potentials given in the caption to Figure 18.

In more general cases without exact recursive feature the associated spin chain is *interactive*. Infinite range interactions might lead to a qualitatively new phenomenon, to a *phase transition* [49] reflected by nonanalyticities in the thermodynamical potentials. (A simple example is provided by a fractal the coverage of which contains a single box with an exponent E_*, while all other box sizes scale with another value $E_0 > E_*$. This leads to $F(\beta) = E_*$ for $\beta > \beta_c$ and $\beta F(\beta) = \beta E_0 - K_0$, otherwise. At $\beta_c = K_0/(E_0 - E_*)$ a first order transition occurs.) A detailed discussion of the phenomenon is beyond the scope of this paper. It is worth noting, however, that methods worked out to handle phase transitions (like transfer matrix, finite size scaling) can successfully be used also in the thermodynamical description of fractals [49], while the eigenvalue formalism mentioned after (54) provides a new technique [46, 44].

16. Relation to the Multifractal Spectrum – the Gibbs Potential

It is clear from the definition (52)–(54) that both $S(E)$ and $F(\beta)$ reflect purely geometrical properties of the fractal. They have, therefore, a priori nothing to do with the multifractal spectrum characterizing also a distribution on the fractal. For an important class of fractal measures, however, $f(\alpha)$ can be shown to be closely related to $S(E)$.

Let us consider measures * with the following property: the probability inside a box is proportional to a power σ of the box size ($-\infty<\sigma<\infty$) for all boxes [41, 44, 45]. By taking into account normalization this means

$$P_J \equiv P(\{s_i\}) = \frac{\varepsilon_J^\sigma}{\sum_J \varepsilon_J^\sigma} \sim e^{\sigma F(\sigma) n - \sigma E_J n}. \tag{60}$$

σ is a parameter of the measure. The crowding index (38) for boxes with a certain value of E is thus

$$\alpha = \sigma - \sigma F(\sigma)/E, \tag{61}$$

i.e. a unique function of E. The number of boxes with a given α (or E) must behave as a power of $\varepsilon = \exp(-E n)$:

$$e^{S(E) n} \sim (e^{-E n})^{-f(\alpha)} \tag{62}$$

from which

$$f(\alpha) = \left.\frac{S(E)}{E}\right|_{E=\frac{\sigma F(\sigma)}{\sigma-\alpha}} \tag{63}$$

follows. In such cases, therefore, the entropy function uniquely *specifies* the $f(\alpha)$ spectrum. Geometrical multifractality as defined in Sect. 13 corresponds to the choice $\sigma = d$. Figure 19 exhibits the $f(\alpha)$ spectra obtained in this way for a few values of σ in the case of the snowflake fractal shown on Figure 9.

When the probabilty of a box depends on the size in a more complicated way than power law, $S(E)$ is *no* longer related to $f(\alpha)$ in any simple manner. It is then worth including also powers of the *probabilities* $P_J \equiv P(\{s_i\})$, i.e. the measures of boxes specified by $\{s_i\}$, into a partition sum [16, 36, 43, 47]. Let us consider

$$\sum_J P_J^p \varepsilon_J^\beta = \sum_{\{s_i\}} P^p(\{s_i\}) s^\beta(\{s_i\}) \sim e^{-\beta G_P(\beta, p) n}, \tag{64}$$

where $-\infty<p<\infty$. In the language of statistical mechanics this is the analogue of an *isoterm-isobar* ensemble [48]. The parameter p is the "*pressure*", $-\ln P_j$ plays the role of a fluctuating *volume* divided by the temperature, and $G_P(\beta, p)$ represents the *Gibbs potential* per spin. The subscript P is to remind us that the potential now depends on the *distribution*.

The free energy is recovered from the Gibbs potential for $p=0$. A completely different characteristic of purely probabilistic nature is the sum $\sum_J P_J^q$, $-\infty<q<\infty$. Since the distribution P_J is normalized, the sum scales with n [50] as

$$\sum_J P_J^q \sim e^{(1-q) K_q n}, \tag{65}$$

which defines a new set of parameters, that of the K_q's. Using the terminology of dynamical systems, we call K_q the *order q generalized entropy* [50] with respect to the distribution P. (The $q=0$ case corresponds to the topological entropy.) From (64) and (65)

$$\beta G_P(\beta, p)\Big|_{\substack{\beta=0\\p=q}} = (q-1) K_q. \tag{66}$$

Thus, the spectra $\beta F(\beta)$ and $(p-1) K_p$ are obtained as restrictions of $\beta G_P(\beta, p)$ on two orthogonal axes $p=0$ and $\beta=0$, respectively. To determine the multifractal spectrum some intermediate point of the $\beta-p$ plane is needed: Using again the fact that fractals are asymptotically selfsimilar and recalling (48) (with $p_j = P_j$, $r_j = \varepsilon_j$, $N = W(n)$) we obtain

$$\beta G_P(\beta, p)\Big|_{\substack{\beta=(1-q) D_q\\p=q}} = 0 \tag{67}$$

as an implicit equation for the spectrum of generalized dimensions D_q with respect to the measure P. Equations (66), (67) are extensions of (55), (56). They mean that D_q and K_q can be obtained from the plot $\beta G_P(\beta, q)$ vs. β by cutting it with the horizontal and vertical axes, respectively. In view of this, the two important spectra D_q and K_q appear only as *partial* characterizations of a fractal measure, a much richer description of which is given by the Gibbs potential $G_P(\beta, p)$ itself. Figure 18 b shows also plots of the potential $\beta G_P(\beta, p)$ at fixed values p for a distribution having an exact recursive structure, as defined in Sect. 12, on the two-scale snowflake fractal.

It is worth noting that for measures of type (60)

$$\beta G_P(\beta, p) = (\beta + \sigma p) F(\beta + \sigma p) - \sigma p F(\sigma), \tag{68}$$

and

$$\beta F(\beta)\,|_{\beta=(1-q) D_q + \sigma q} = q \sigma F(\sigma), \tag{69 a}$$

$$K_q = \frac{\sigma q}{q-1}(F(\sigma q) - F(\sigma)), \tag{69 b}$$

i.e. all quantities can be expressed in terms of the free energy alone.

Distributions on one-scale fractal supports from another interesting special class. Such cases are characterized by a single energy value E_0, and consequently

$$\beta G_P(\beta, p) = \beta E_0 + (p-1) K_p, \tag{70}$$

* Called Gibbs measures in dynamical systems [39].

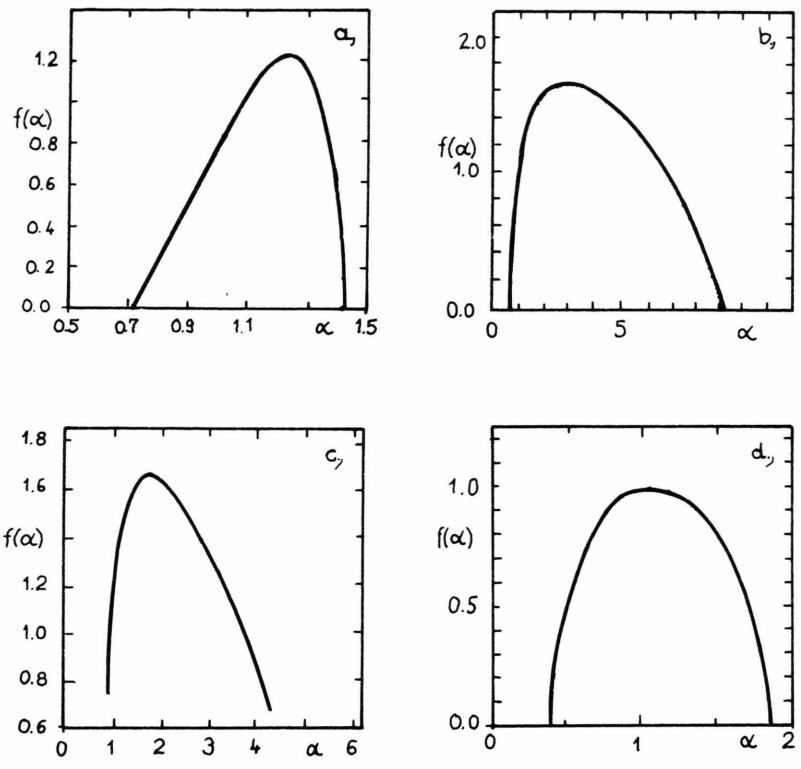

Fig. 20. Multifractal spectra for different systems, a qualitative sketch obtained by using the results of [53–56]. – a) $f(\alpha)$ with respect to the natural measure for the Hénon attractor [53]. – b) $f(\alpha)$ with respect to the growth probability for DLA measured on a growing ammonium chlorid crystal [54]. – c) $f(\alpha)$ with respect to the voltage distribution for a percolating cluster in a random resistor network [55]. – d) The multifractal spectrum along a straight line cutting through the support of energy dissipation in fully developed turbulence as measured in [56].

i.e. the plot $\beta G_P(\beta, p)$ vs. β is a staight line for all fixed p. From (67) the explicit relation $E_0 D_q = K_q$ follows then between dimensions and entropies. The example of Sect. 9 belongs to this class with $E_0 = \ln 3$.

Finally, we mention that there is an essential difference in calculating the multifractal spectrum via (39), (40) and via the thermodynamical formalism. When introducing D_q and $f(\alpha)$ we used a *uniform* grid. The organization of the fractal, however, defines a range of length scales and a coverage of the set by *boxes of different size*. This is why the equations specifying the multifractal spectrum appear now in different forms. The knowledge of the encoding helps to find an "optimal" coverage which is optimal also in the sense that the asymptotic regime in n is reached for this coverage much faster than by refining a uniform grid. In other words, the application of the thermodynamical formalism provides an increased *precision* in describing the scaling properties of multifractals. In particular, this is the case at phase transition points, which are very difficult to locate by means of other methods.

IV. Closing Remarks

Although it is not been the aim of this report to give a complete overview of what has been done on the field of fractals and multifractals, it is worth illustrating the wide range of recent applications in natural phenomena by few examples. We do not go into a detailed discussion of the results since many of them have recently been reviewed [51, 52, 8, 9]. Rather we give here a pictorial comparison of $f(\alpha)$ spectra obtained for different systems in numerical or laboratory experiments (Fig. 20) [52–56].

In the case of *chaotic* motion the most important distribution on strange attractors is the so-called *natural measure* [26], the distribution describing how often a given part of the attractor is visited by chaotic trajectories, in the long time limit. This defines a fractal measure, which under special conditions [40, 41, 44, 45] can be also of type (60). The field of dynamical systems is the one where the thermodynamical formalism has successfully been applied. Recent for-

mulations are based on the set of all unstable *periodic orbits* [57, 53] which can uniquely be encoded. Phase transitions have been found to be *typical* for chaotic attractors [49]. Figure 20a exhibits the $f(\alpha)$ spectrum for the Hénon attractor, in which a straight line segment, the sign of a phase transition, can clearly be seen [53].

In growth phenomena, like *DLA* [24, 30, 31] the *growth probability* distribution on the cluster is a fractal measure. The broad range of the crowding index observed (Fig. 20b) [54] is a consequence of the fact that the distribution is concentrated on the tips and the bulk is practically screened. The maximal α value is, therefore, rather large.

A quite different example is that of the *voltage distribution* on the backbone of a *percolating* cluster in a random resistor network [29, 55]. The range of α values is narrower than that for the DLA [55], but the shape of the middle parts of the two spectra is similar (Figure 20c). Note that the spectrum for the voltage distribution does not go down to zero. At the right end this is the consequence of the numerical procedure: $\alpha_{-\infty}$ could not be reached in the simulation of [55]. The positivity of f at the left end is, however, essential: the so-called single connected bonds, carrying the total current, and consequently maximal voltage, form a set of nonzero fractal dimension [55].

In the case of fully developed *turbulent* flows of incompressible fluids the distribution of the *energy dissipation* has been pointed out to be a multifractal [27, 32]. The $f(\alpha)$ spectrum exhibited on Fig. 20d differs from the previous ones in the property that it was obtained for a one-dimensional *section* along the flow [56] with the assumption that the support of dissipation was an isotropic fractal.

The complete Fig. 20, thus, illustrates the differences (and similarities) in the multifractal spectra characterizing different natural phenomena.

Finally two remarks are in order.

The thermodynamical formalism has not yet been applied outside the field of dynamical systems. The accuracy of the results obtained in other cases could not reach the level which is expected to be provided by the use of the thermodynamical formalism. Furthermore, the existence of phase transitions can hardly be pointed out by means of other methods. Therefore, the following recent finding is of interest: certain fractal measures on Julia sets arising in dynamical systems exhibit quantitative similarity to the growth probability distribution on DLA clusters [58]. This observation might help in *enlarging* the range of natural phenomena where the thermodynamical formalism can be applied with success.

As illustrated also by Fig. 20, measurements have concentrated on the $f(\alpha)$ spectrum so far. In cases where the encoding is known, it would be, however, desirable to evaluate the complete *thermodynamical potentials* $F(\beta)$ or $G_P(\beta, p)$ since they contain *more* information about the fractal or multifractal than the dimensions. Their knowledge might also make a stronger *classification* of systems possible than that provided by the multifractal spectrum $f(\alpha)$ alone.

Appendix (to Section 9)

Since m_1 is expected to be large for $n \gg 1$, Stirling's formula

$$\ln k! = k(\ln k - 1),$$

$k \gg 1$, can be used when evaluating $\ln N_m P_m$. One, thus obtains

$$\ln N_m P_m = n \ln n - m \ln m - (n-m) \ln (n-m) + m \ln 2 + m \ln p_1 + (n-m) \ln p_2 .$$

The maximum of this expression is found to be at m_1 given by (27). The value of $\ln N_{m_1} P_{m_1}$ is then 0 with the accuracy of Stirling's formula. It is easy to see that

$$\ln N_{m_1} = -n(2 p_1 \ln p_1 + p_2 \ln p_2),$$

from which (28) and (29) follow.

The calculation of f_q goes along similar lines.

Acknowledgements

The author is indebted for valuable discussions and collaboration with T. Bohr and I. Procaccia. He acknowledges a correspondence with B. Mandelbrot. Thanks are due to I. Szilágyi for paying his attention to [1], and to A. Csordás, T. Geszti, J. Kertész, I. Kondor, Z. Kovács, G. Marx, Z. Rácz, L. Sasvári, G. Szabó, P. Szépfalusy, and T. Vicsek for useful comments and a cirital reading of the manuscript at different stages of its preparation. The author thanks the Referee for suggesting the inclusion of a chapter on the thermodynamical formalism and for further stimulating remarks. This work was supported by grants provided by the Hungarian Academy of Sciences (Grants No. AKA 283.161 and OTKA 819).

[1] W. F. Ganong, Review of Medical Physiology, 8th Ed. Lange Medical Publications, California 1977.
[2] B. B. Mandelbrot, Les Object Tractals, Flammarion, Paris 1975. – B. B. Mandelbrot, Fractals: Form, Chance, and Dimension, Freeman, San Francisco 1977. – B. B. Mandelbrot, The Fractal Geometry of Nature, Freeman, San Francisco 1982.
[3] K. J. Falconer, The Geometry of Fractal Sets, Cambridge Univ. Press, Cambridge 1985.
[4] N. Ostrowsky and H. E. Stanley (eds.), On Growth and Form: Fractal and Non-Fractal Patterns in Physics, M. Nijhoff, The Hague 1985.
[5] L. Pietronero and E. Tosatti (eds.), Fractals in Physics, North-Holland, Amsterdam 1986.
[6] E. Mayer-Kress (ed.), Dimensions and Entropies in Chaotic Systems, Springer, New York 1986.
[7] H. O. Peitgen and P. Richter, The Beauty of Fractals, Springer, New York 1986.
[8] J. Feder, Fractals, Plenum Press, New York 1988.
[9] T. Vicsek, Fractal Growth Phenomena, World Scientific, Singapore 1988, to appear.
[10] G. Cantor, Mathematische Annalen **21,** 545 (1883).
[11] J. D. Farmer, in Ref. [6].
[12] D. K. Umberger and J. D. Farmer, Phys. Rev. Lett. **55,** 661 (1985). – C. Grebogi, S. W. McDonald, E. Ott, and J. A. Yorke, Phys. Lett. **110 A,** 1 (1985). – D. K. Umberger, G. Mayer-Kress, and E. Jen, in Ref. [6]. – R. Eykholt and D. K. Umberger, Physica **D 30,** 43 (1988).
[13] H. von Koch, Arkiv för Matematik, Astronomi och Fysik **1,** 681 (1904).
[14] T. Vicsek, J. Phys. **A 16,** L 647 (1983).
[15] H. G. E. Hentschel and I. Procaccia, Physica **D 8,** 435 (1983).
[16] T. C. Halsey, M. H. Jensen, L. P. Kadanoff, I. Procaccia, and B. I. Schraiman, Phys. Rev. **A 33,** 1141 (1986).
[17] T. Tél and T. Vicsek, J. Phys. **A 20,** L 835 (1987).
[18] M. V. Berry and Z. V. Lewis, Proc. Roy. Soc. London **A 370,** 459 (1980).
[19] B. B. Mandelbrot, in Ref. [5].
[20] K. Weierstrass, Mathematische Werke, Mayer and Müller, Berlin 1895.
[21] J. L. Kaplan, J. Mallet-Paret, and J. A. Yorke, Ergod. Theor. Dynam. Systems **4,** 261 (1984).
[22] R. F. Voss, in: Scaling Phenomena in Disordered Systems (R. Pynn and A. Skjeltorp, eds.), Plenum, New York 1985.
[23] D. Stauffer, Introduction into Percolation Theory, Taylor and Francis, London 1985.
[24] P. Meakin, in: Phase Transitions and Critical Phenomena, Vol. 12 (C. Domb and J. Lebowitz, eds.), Academic Press, New York 1988.
[25] J. Kertész, Phil. Mag. **B 56,** 729 (1987).
[26] H. G. Schuster, Deterministic Chaos, Physik Verlag, Weinheim 1984. – J. P. Eckmann and D. Ruelle, Rev. Mod. Phys. **57,** 617 (1985). – P. Grassberger, in: Chaos (A. V. Holden, ed.), Manchester University Press, Manchester 1986.
[27] B. B. Mandelbrot, J. Fluid Mech. **62,** 331 (1974).
[28] N. Ghil, R. Benzi, and G. Parisi (eds.), Turbulence and Predictability of Geophysical Flows and Climate Dynamics, North Holland, Amsterdam 1985.
[29] A. Coniglio, Physica **140 A,** 51 (1986). – L. de Arcangelis, S. Redner, and A. Coniglio, Phys. Rev. **B 31,** 4725 (1985).
[30] T. C. Halsey, P. Meakin, and I. Procaccia, Phys. Rev. Lett. **56,** 854 (1986).
[31] C. Amitrano, A. Coniglio, and F. di Liberto, Phys. Rev. Lett. **57,** 1016 (1986). – Y. Hayakawa, S. Sato, and M. Matsushita, Phys. Rev. **A 36,** 1963 (1987).
[32] U. Frisch and G. Parisi, in Ref. [28]. – R. Benzi, G. Paladin, G. Parisi and A. Vulpiani, J. Phys. **A 17,** 3521 (1984).
[33] B. B. Mandelbrot, Fractals and Multifractals: Noise Turbulence and Galaxies, Springer, New York 1988, to appear.
[34] D. Farmer, Z. Naturforsch. **37 a,** 1304 (1982).
[35] A. Rényi, Probability Theory, North Holland, Amsterdam 1970.
[36] P. Grassberger, Phys. Lett. **97 A,** 227 (1983); **107 A,** 101 (1985).
[37] J. Balatoni and A. Rényi, Publications of the Math. Inst. of the Hungarian Acad. Sci **1,** 9 (1956) (in Hungarian); English translation in: The Selected Papers of A. Rényi, Vol. 1, p. 558, Akademiai, Budapest 1976. – D. Farmer, E. Ott, and J. A. Yorke, Physica **D 7,** 153 (1983).
[38] R. E. Amritkar, A. D. Gangal, and N. Gupte, Phys. Rev. **A 36,** 2850 (1987).
[39] Y. Sinai, Russ. Math. Surv. **166,** 21 (1972). – R. Bowen, Lecture Notes in Math. **470,** 1 (1975). – D. Ruelle, Thermodynamic Formalism, Addison-Wesley, Reading 1978.
[40] M. J. Feigenbaum, M. H. Jensen, and I. Procaccia, Phys. Rev. Lett. **57,** 1503 (1986). – M. H. Jensen, L. P. Kadanoff, and I. Procaccia, Phys. Rev. **A 36,** 1409 (1987). – M. J. Feigenbaum, J. Stat. Phys. **46,** 919, 925 (1987).
[41] T. Bohr and D. Rand, Physica **25 D,** 387 (1987).
[42] P. Szépfalusy and T. Tél, Phys. Rev. **A 34,** 2520 (1986). – T. Tél, Phys. Rev. **A 36,** 2507 (1987). – P. Collet, J. Lebowitz, and A. Porzio, J. Stat. Phys. **47,** 609 (1987). – A. Arneodo and M. Holschneider, J. Stat. Phys. **50,** 995 (1988). – J. Bene and P. Szépfalusy, Phys. Rev. **A 37,** 1703 (1988). – A. Csordás and P. Szépfalusy, Phys. Rev. A **38,** 2582 (1988).
[43] R. Badii, Thesis, Zürich 1987.
[44] T. Bohr and T. Tél, The Thermodynamics of Fractals, in: Directions in Chaos, Vol. 2 (Hao Bai-Lin, ed.), World Scientific, Singapore 1988.
[45] D. Bessis, G. Paladin, G. Turchetti, and S. Vaienti, J. Stat. Phys. **51,** 109 (1988). – S. Vaienti, J. Phys. **A 21,** 2313 (1988).
[46] M. J. Feigenbaum, I. Procaccia, and T. Tél, The Scaling Properties of Multifractals as an Eigenvalue Problem, preprint 1988. – M. J. Feigenbaum, J. Stat. Phys. **52,** 527 (1988).
[47] M. Kohmoto, Phys. Rev. **A 37,** 1345 (1988).
[48] A. Münster, Statistical Thermodynamics, Springer, New York 1969.
[49] P. Cvitanović, in: XV. Int. Coll. on Group Theoretical Methods in Physics (R. Gilmore, ed.), World Scientific, Singapore 1987. – R. Badii and A. Politi, Phys. Scripta **35,** 243 (1987). – D. Katzen and I. Procaccia, Phys. Rev. Lett. **58,** 1169 (1987). – P. Szépfalusy, T. Tél, A. Csordás, and Z. Kovács, Phys. Rev. **A 36,** 523 (1987). – T. Bohr and M. H. Jensen, Phys. Rev. **A 36,** 4904 (1987). – P. Grassberger, R. Badii, and A. Politi, J. Stat. Phys. **51,** 135 (1988); J. Phys. **A 21,** L 763 (1988).
[50] P. Grassberger and I. Procaccia, Physica **D 13,** 34 (1984).
[51] H. E. Stanley and P. Meakin, Nature **335,** 405 (1988). – I. Procaccia, Nature, to appear.
[52] G. Paladin and A. Vulpiani, Phys. Rep. **156,** 147 (1987).
[53] G. H. Gunaratne and I. Procaccia, Phys. Rev. Lett. **59,** 1377 (1987).
[54] S. Ohta and H. Honjo, Phys. Rev. Lett. **60,** 611 (1988).
[55] L. de Arcangelis, S. Redner, and A. Coniglio, Phys. Rev. **B 34,** 4656 (1986).
[56] C. Meneveau and K. R. Sreenivasan, Phys. Rev. Lett. **59,** 1424 (1987).

[57] D. Auerbach, P. Cvitanović, J. P. Eckmann, G. H. Gunaratne, and I. Pocaccia, Phys. Rev. Lett. **58,** 2387 (1987). – T. Kai and K. Tomita, Prog. Theor. Phys. **64,** 1532 (1980). – Y. Takahashi and Y. Oono, Prog. Theor. Phys. **71,** 851 (1984). – H. Fujisaka and M. Inoue, Prog. Theor. Phys. **77,** 1334 (1987). – T. Morita, H. Hata, H. Mori, T. Horita, and K. Tomita, Prog. Theor. Phys. **78,** 511 (1987); **79,** 296 (1988). – H. Hata, T. Morita, K. Tomita, and H. Mori, Prog. Theor. Phys. **78,** 721 (1987). – C. Grebogi, E. Ott, and J. Yorke, Phys. Rev. **A 36,** 3522 (1988); Phys. Rev. **A 37,** 1711 (1988). – P. Cvitanović, G. H. Gunaratne, and I. Procaccia, Phys. Rev. A **38,** 1503 (1988).

[58] I. Procaccia and R. Zeitak, Phys. Rev. Lett. **60,** 2511 (1988). – T. Bohr, P. Cvitanović, and M. H. Jensen, Europhys. Lett. **6,** 445 (1988).

Verantwortlich für den Inhalt: A. KLEMM
Satz und Druck: Konrad Triltsch, Würzburg